Initial Flight Experiments of a Canopy Sampling Aerial Manipulator

James R. Kutia, Karl A. Stol, Weiliang Xu
Department of Mechanical Engineering
University of Auckland
Auckland, New Zealand
jkut003@aucklanduni.ac.nz

***Abstract*— Development of an aerial manipulator prototype for canopy sampling is presented. As part of addressing the unique challenges of operating in a forest canopy environment, the prototype features an offset-mounted manipulator. The first steps of flight experiments have been conducted in an attempt to determine the viability of an off-the-shelf PID flight control implementation – acceptable performance would negate the need to use more complex implementations. Indoor testing has been conducted with the aid of motion capture in-the-loop to alleviate inertial sensing uncertainties. This work investigates the two simplest dynamic phases of a sampling operation: position holding during free-flight, and whilst the arm is moving.**

***Keywords*— aerial manipulation, manipulator, robotic arm, UAV, unmanned aerial vehicle, canopy sampling, forestry**

I. Introduction

Aerial manipulation using an unmanned aerial vehicle (UAV) can generally be defined as intentional physical interactions with the environment in order to achieve some goal or task. Previous studies to date have taken several forms, which can be distinguished based on their dynamic natures: load carrying (including grippers) [1-3], surface interactions for contact inspection [4, 5] and multi DoF manipulation - typically using some form of robot arm [6, 7]. Even in its infancy, several examples of specific case studies demonstrate the potential of this research, such as valve turning [8] and the opening and closing of drawers [9]. Nonetheless, it is acknowledged that real-world applicability of manipulation tasks is heavily dependent on robotic perception research such as obstacle avoidance, and alongside modelling and control, this accounts for most other aerial manipulation research [10, 11].

The research presented here has been driven by the application of upper canopy sampling, specifically of Pinus radiata plantations which are the most abundant commercial species in New Zealand. In summary, the need for physical samples (specifically pine needles) arises when testing for pathogens and diseases, genetic work, breeding etc.; therefore only small sections of outlying branches are taken (≈ 10 cm length) which makes this well-suited for employment of aerial robotics. This is a great improvement on labour intensive methods presently used - the standard method for sample retrieval in NZ is by use of a shotgun projectile to break a random set of branches off.

A detailed introduction to the problem has been presented previously, along with initial modelling and simulation work [12]. These results have suggested that a PID-based control architecture can successfully govern attitude and position whilst subjected to the disturbances imposed by manipulator movement and tree branch interactions. Based on these results, the work presented here aims to experimentally investigate canopy sampling operations under a system of PID loops controlling the aircraft and manipulator. Although related works have focused on the derivation of modern controllers, such as sliding mode [13] and model-reference adaptive control [14], it would be beneficial to determine whether a conventional PID control structure meets canopy sampling control objectives before looking at more complex control laws; this reasoning has been shared by previous work using a rotorcraft to capture and transport loads [15].

The paper will first describe the canopy sampling aerial manipulator (CSAM) prototype that has been developed, with reference to the scenario features it addresses. A brief overview is given of the PID control architecture under investigation. Lastly, the PID analysis itself is conducted through as a series of flight experiments.

II. Aerial Manipulator Prototype

The CSAM prototype, pictured in Figure 1, is described in terms of it 3 main subsystems: aircraft, manipulator and on-board intelligence. Relevant system parameters are given in Table I.

In terms of system architecture, a mini PC is fixed on-board to run computationally expensive programs such as manipulator path planning, and branch tracking (as part of future work). Robot Operating System (ROS) is used as it is well-suited for running and communicating between the different CSAM processes. Low level flight controllers are isolated via the dedicated flight control board; this safeguards the aircraft if there is some software or hardware failure of the mini PC as it always remains controllable via radio. All devices communicate with the PC.

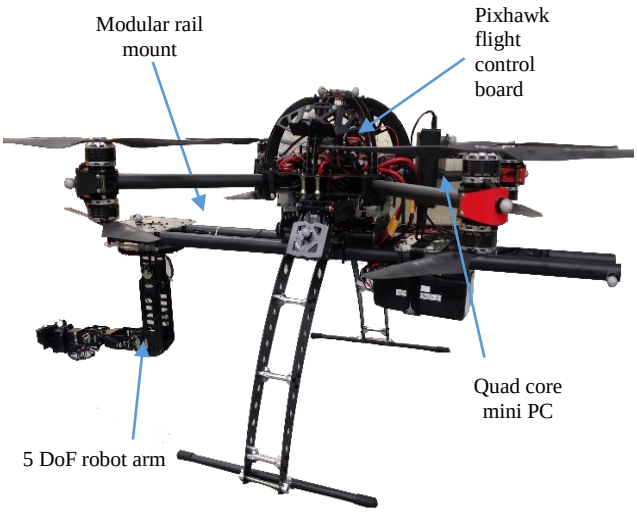

Fig. 1. CSAM prototype

TABLE I. CSAM PHYSICAL PARAMETERS

Property	**Value**
CSAM Mass	Aircraft: 5.77 Kg Manipulator: 1.30 Kg Mount Rail Asm: 0.56 Kg Batteries: 2.6 Kg *Total: 10.23 Kg*
Propeller Size	17 x 5.8”
Thrust	3.85 Kg/motor × 8 = 30.8 Kg
Frame Diameter (including propellers)	0.85 m (1.28 m including prop)
Maximum Extension	0.41 m
Arm Lift Capacity (@ max extension)	0.5 Kg
Joint Speed (software limited)	90 deg/s

A. *Aircraft*

Manipulation applications inherently require ample excess thrust to carry the manipulating mechanism and reject environmental interaction disturbances. The CSAM is based on an off-the-shelf coaxial octorotor. Compared with a typical quadrotor, eight rotors provide redundancy in the event of a single failure. The coaxial configuration was preferred to planar because shorter boom lengths can be used for a given propeller size, thus giving a smaller footprint area for a given thrust; reducing the footprint is important because it means the aircraft can operate in more confined spaces, thus reducing the chance of collisions with surrounding branches when operating in the vicinity of the forest canopy; furthermore, wind disturbances decrease with cross-sectional area. Table I gives a power-to-weight figure of 3, which is considered underpowered for a typical multirotor, however given the aircraft will be operating at, or near hover state, this is acceptable.

A main design feature from Figure 1 is the large arm offset in front of the aircraft. It is acknowledged that for optimal dynamic performance, the arm should be mounted as close to the center as possible to minimize changes in the center of mass. However, the arm base is purposely offset by 0.45 m such that it lies approximately in line with the prop tips. This is justified by considering Figure 2, which depicts potential samples on a typical pine tree top. Here, branches *1* and *2* are accessible from the top (assuming no other trees inhibit the CSAM), whereas branches *3* and *4* must be approached from the side. This side is only possible if the arm can reach beyond the aircraft. Therefore a tradeoff must be made between CoM and reachability. Note that a static balance is achieved whilst the arm is in a stowed position by using the batteries as a counterweight. Previous work has used an active sliding mechanism to achieve balance as a function of manipulator position [6], and one purpose of this study is to determine whether such a feature is required for this system. It is expected that the arm offset will be modified based on findings from future experiments.

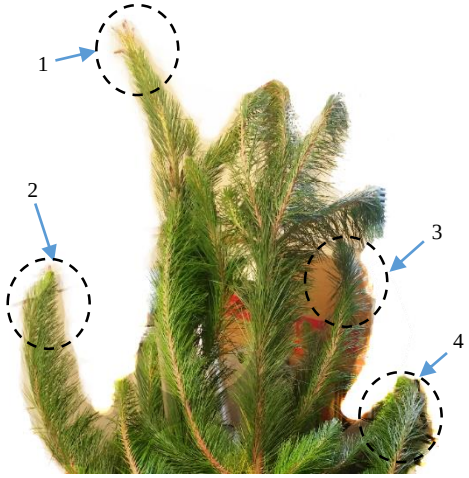

Fig. 2. Representative Pinus radiata specimen: top 2 m section from a 6 m tall tree

B. *Manipulator*

An off-the-shelf 5 DoF robot arm is used on the aircraft for sampling; Figure 3 illustrates the joints, termed pan, shoulder, elbow, wrist and wrist rotate. Dynamixel robotic smart servos are employed as actuators because inbuilt PID controllers and current sensors assist system modularity and allow easy control of position, velocity and torque – with the latter allowing a crude form of active compliance.

From Table I, the system payload is governed by the arm capacity, which is 0.5 Kg at full extension; this fulfils requirements, considering a typical branch sample specimen measuring 10 cm in length weighs ≈ 0.15 Kg. The manipulator cannot achieve an arbitrary orientation and position as it does not have 6 DoF; it is hypothesized that this is not an issue as it will be gripping a cylindrical branch, which can be done at any angle around its circumference. However, the yaw motion of the aircraft can be exploited as an extra DoF if necessary, where the fixed offset between aircraft geometric center and manipulator base forms a new link.

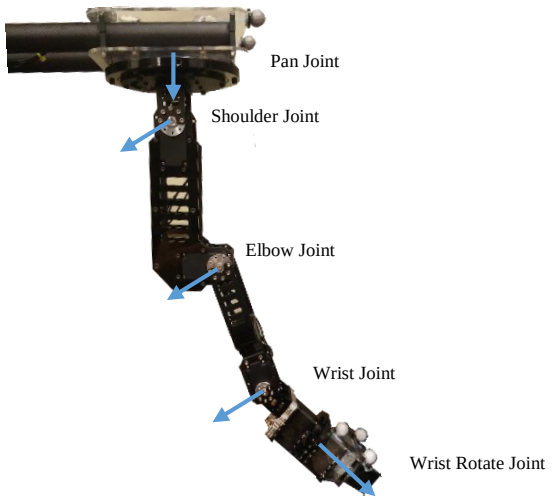

Fig. 3. 5 DoF manipulator mechanism

For the purpose of this study, the original gripper is retained, however as experiments progress, a custom sampling mechanism is proposed as part of future work.

III. System Control Implementation

A. Aircraft

The primary contribution of this study is investigating performance of a PID-based control implementation for conducting canopy study. An advantage of this approach is that it is used by most off-the-shelf UAV solutions, and therefore requires fewer modifications to facilitate aerial manipulation. In this case, APM:Copter open-source firmware has been used with a Pixhawk flight control board. The flight controllers are comprised of a series of cascaded PID control loops, which can be broadly split into two sections: low-level attitude control, and high-level position control; these are illustrated in an abbreviated form in Figures 4 and 5. It can be seen that the highest level set-point, a desired inertial position, propagates through the series of cascaded controllers, resulting in a desired roll and pitch angle to achieve/maintain this position. This is then fed into the attitude controllers, which generate the final control output – individual motor speeds. This work is concerned with position holding performance, which is therefore a function of attitude and position controller performance. The figures also show motion capture replaces the standard fusion of IMU data with GPS, in accordance with the experimental setup.

System performance will be limited by the quality of gain tuning. For this work, gains were tuned using a heuristic approach due to time constraints. The manipulator was kept in a stowed position, and roll/pitch commands given to the aircraft; angle and rate controller gains were adjusted by analysing the response. Position and position rate controllers were left at default gains.

B. Manipulator

Dynamixel smart servos are driven by inbuilt microcontrollers, which use a series of PID controllers to govern joint position, speed and torque; these desired states are communicated over a serial link. Control performance has obviously been proven as an off-the-shelf product, with negligible error when compared with the relative motion of the aircraft in inertial space. Hence it can be assumed that computed joint trajectories will result in high precision positioning of the end effector.

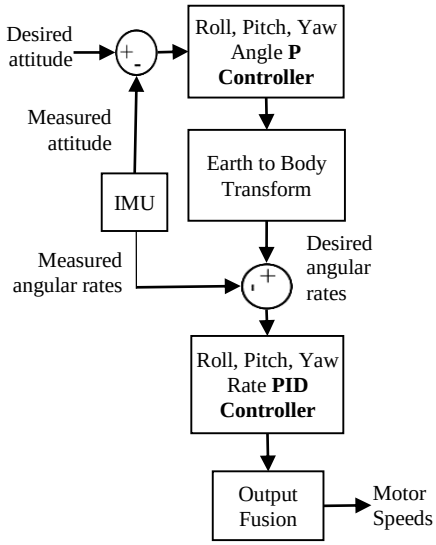

Fig. 4. ArduCopter attitude control

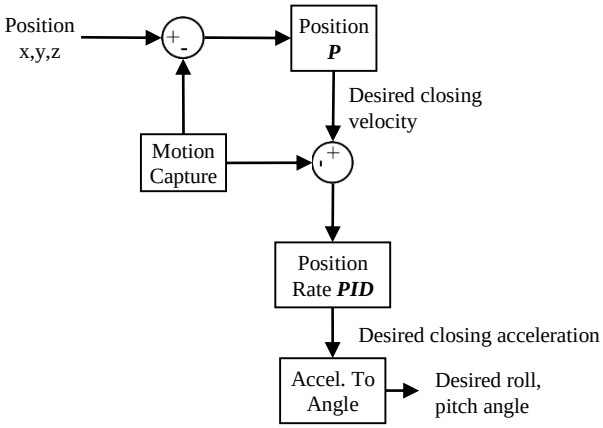

Fig. 5. ArduCopter position control

IV. Experiments

In order to investigate control system performance in the context of canopy sampling, testing must be conducted with respect to the different dynamic phases of flight: free-flight, robot arm movement, tree-branch coupling and tree-branch decoupling (cutting) – these are discussed in previous work [12]. By working in the order above, further disturbances are added to the system; for example, an aircraft in free flight is only subject to its own dynamics, and aerodynamic influences such as wind and ground effect. Arm movement adds both static and dynamic disturbances, the latter of which can be reduced by moving the arm slowly. Finally, the effect of tree branch coupling and decoupling is best found through experimentation due to inherent natural variability. This work presented here covers initial experiments in free-flight and arm movement.

A. *Setup and Criteria*

In order to truly evaluate the PID control system performance, all acquired sensor data should be as near-perfect as possible; in the case of UAV's, greatest sensor errors occur in the inertial sensing, which typically relies on GPS. For this reason, initial flight tests have been carried out in a motion capture lab measuring 8 m x 8 m, as illustrated in Figure 6. However, it is acknowledged that by operating indoors, the aircraft is not subjected to realistic outdoor conditions that may affect controller performance, namely wind – which can be turbulent in the vicinity of a forest canopy. Secondly, any flight indoors introduces rotor wake interactions and ground effect; these effects are even more pronounced for a larger aircraft, however they are unavoidable.

Fig. 6. CSAM flight testing setup

Flight performance criteria is defined with respect to canopy sampling operations. The most important goal for any UAV flight controller is to retain stability in the lower level controllers, i.e. attitude control; failure would result in a crash. The focus of the work below is quantifying position-holding performance. The CSAM must be able to approach a branch and retrieve a sampling without drifting into surrounding branches; the system must also track and couple with the chosen branch; this imposes a limit on position tracking errors due to the maximum reach of the manipulator arm, which is 0.41 m. Therefore any drift greater than this distance makes sampling unachievable. Ideally, any drift would not exceed 0.2 m in any direction - this would mean the end effector remains in a central position of its workspace, thus giving it maximum manoeuvrability. Free-flight results are presented first as a way of quantifying some baseline measure of performance.

B. *Free-Flight Position Hold*

For free-flight testing, the aircraft was manually flown to the maximum safe altitude of approximately 2 m to reduce ground effect. At this point, a "loiter" mode was engaged whereby the controllers attempt to keep the aircraft in a constant inertial frame position, with feedback provided from motion capture. The manipulator was kept in its stowed position, whereby the aircraft is statically balanced at a level attitude with the batteries.

First, attitude responses are presented about the roll and pitch axes in Figures 7 and 8. These responses are also important in terms of position hold performance due to the cascaded nature of the control system implementation.

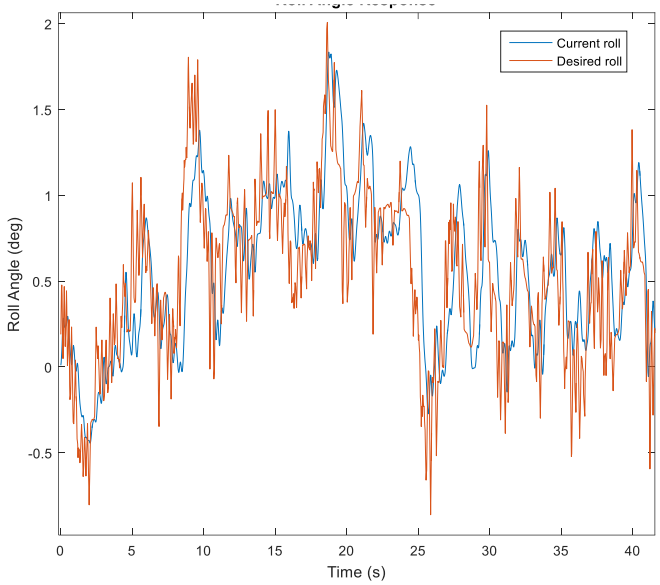

Fig. 7. Free-flight roll response during position hold

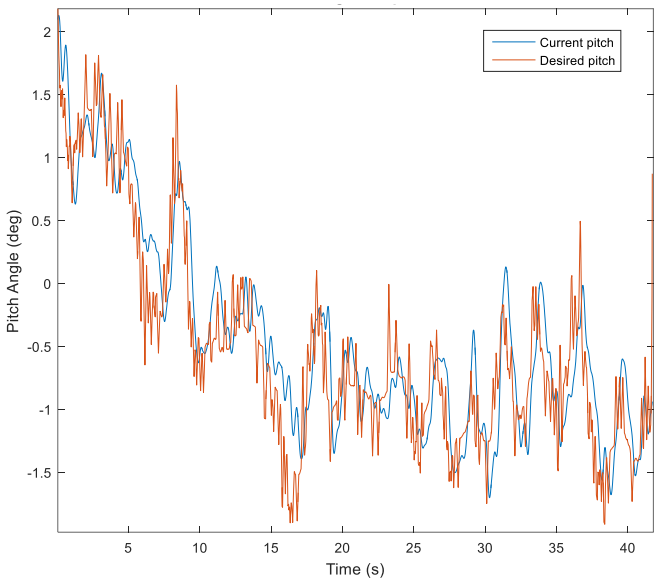

Fig. 8. Free-flight pitch response during position hold

In general, the aircraft response lags the desired trajectory by approximately 0.2 s; there is obvious overshoot in both instances. These are both a result of the higher inertia of the system compared with typically sized UAV's; it also suggests further tuning may be required. The desired roll and pitch angles are clearly biased away from 0, however this is likely due to an IMU calibration error. It is worth mentioning that the magnitude of attitude changes is approximately 3 degrees about each axis. With reference to Figure 5, this means the position controller only outputs a small lean angle, thus the aircraft does not aggressively attempt to correct any position error. This is significant as it may be detrimental to system performance when

disturbances from the manipulator or tree branch are introduced. Again, this can be addressed by tuning the position controller gains.

The position response in each inertial direction is illustrated in Figure 9. Oscillatory responses are also apparent, this is to be expected given the attitude responses seen. With a maximum position magnitude error of approximately 14 cm, the criteria for canopy sampling under free-flight conditions has been met.

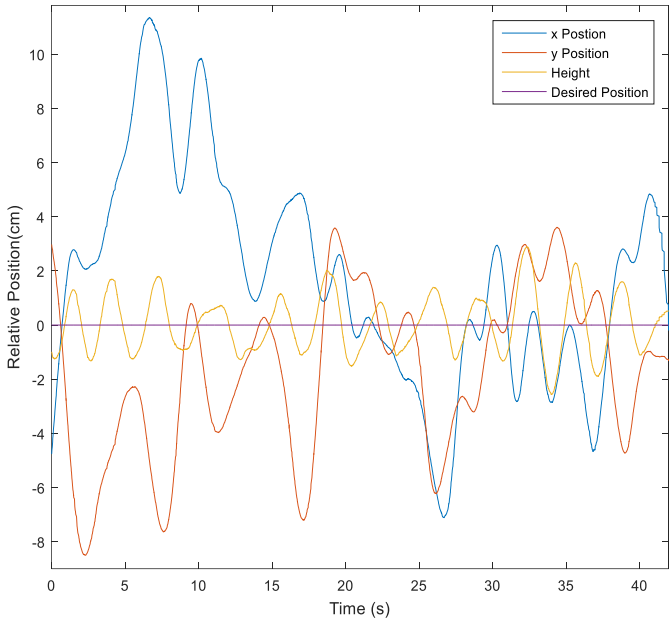

Fig. 9. Free-flight inertial position response during position hold

RMS errors for all free-flight responses are given in Table II, this provides a measure of quantitative comparison with arm-movement experiment results below.

TABLE II. FREE FLIGHT RMS ERRORS

Response Variable	**RMS Error**
Roll	1.48 deg
Pitch	1.47 deg
Position	3.27 cm [4.37 3.44 1.09] cm

C. Free-Flight with Arm Sweep

Methodology for arm sweep testing was identical to free-flight, except obviously the arm was moved along a predefined trajectory. The end effector path was intuitively programmed like “sweep”, as this would provide maximum disturbances to the aircraft due to center of mass offsets:

- Start at stowed position
- Extend to maximum extension in front of the aircraft (40 cm).
- Pan left 90 degrees to maximum extension on the left side of aircraft.
- Pan right 180 degrees to maximum extension on the right side of aircraft.
- Return to center, still at maximum extension.
- Retract end effector to a position 15 cm in front of the manipulator base.

All movements were carried out with a goal Cartesian speed of 5 cm/s, however since no intermediate goal points were defined, this is only an approximation. The joint positions throughout these movements are depicted in Figure 10. The differing line gradients illustrates a range of joint speeds; there are also flat parts to the response, this is because the manipulator was purposely stopped between each movement step to introduce inertial disturbances from accelerations of the joints. Note that the sweep was carried out twice from different initial positions.

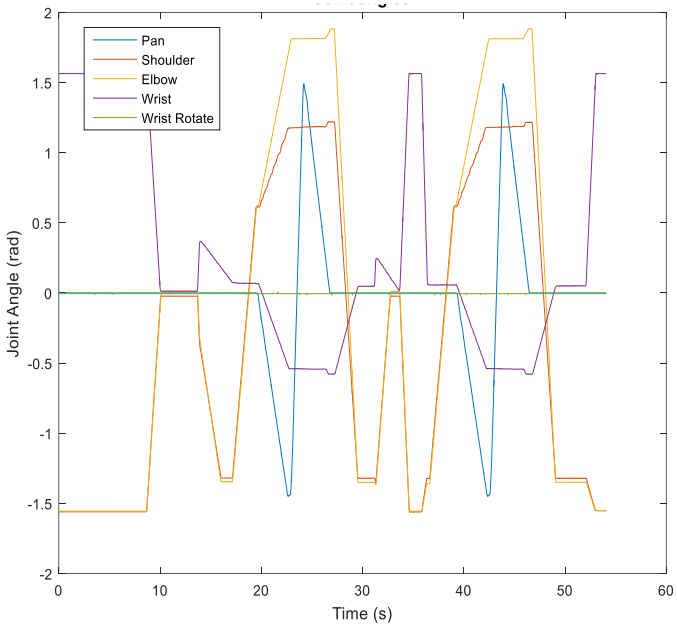

Fig. 10. Joint position trajectories during flight

The effect of this manipulator movement is most pronounced in the roll and pitch responses pictured in Figures 11 and 12. Corrections in attitude are necessary to reject disturbances from the manipulator, and this is the cause of obvious peaks seen. It was also apparent that these disturbances were generated by the transient periods of joint movement, i.e. starting and stopping. This will be considered in future work concerning acceleration and velocity planning.

It can also be seen that the controller commands larger pitch angles than roll; this can be explained by considering the design of the CSAM, whereby the manipulator is located at an offset from the geometric center along the roll axis, but in-line with the pitch and yaw axes. Therefore, any extension of the manipulator in front of the aircraft has a larger effect on aircraft balance as its total displacement is already greater. This means pitch controller gains should be different to roll, yet in this testing they were made identical. Interestingly, Table III shows equal RMS errors in roll and pitch, thus suggesting the controller is able to compensate for the manipulator offset.

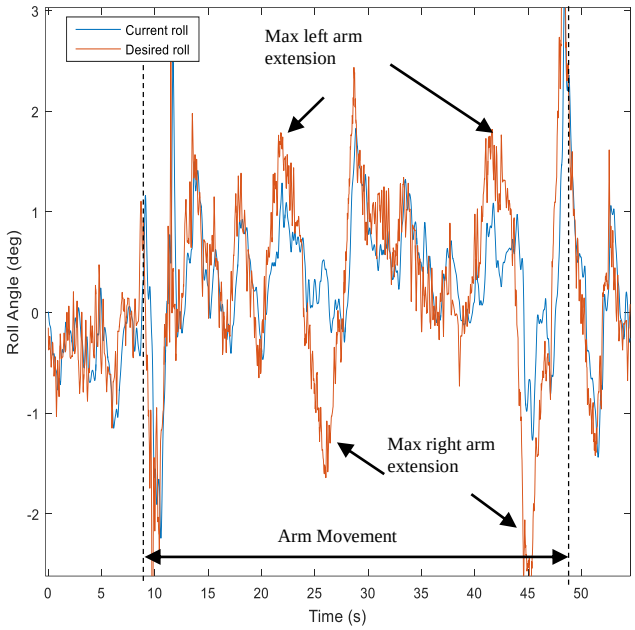

Fig. 11. Position hold roll response, with manipulator movement

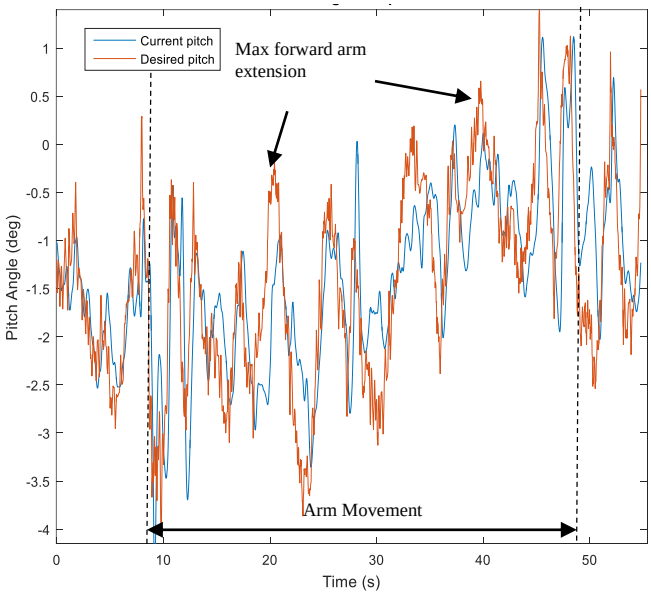

Fig. 12. Position hold pitch response, with manipulator movement

Figure 13 shows a similar oscillatory response to the free-flight results in Figure 9. Large deviations in position occur at the same times as those in pitch and roll, due to transient motion of the joints. The x position error (along the roll axis) is seen to peak at approximately 18 cm during the last stages of arm movement; although this lies within the aforementioned criteria, this is far from ideal performance. As a consequence of these spikes, the RMS position error compared with free-flight almost doubled to 5.86 cm, with the worst performance along the x axis – as expected.

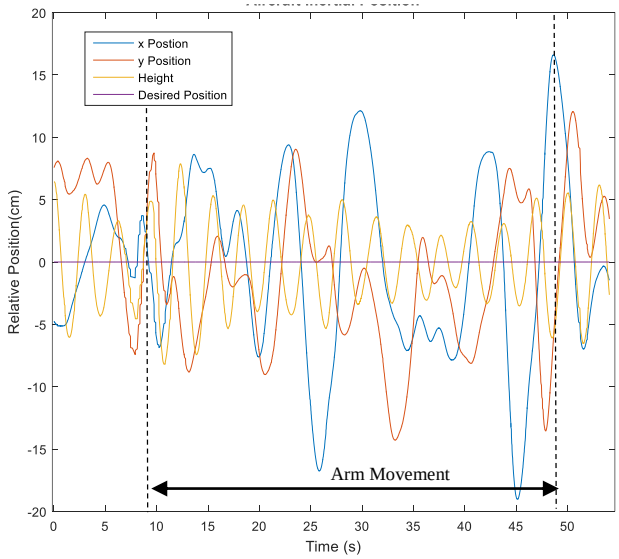

Fig. 13. Inertial position response during position hold, with manipulator movement

TABLE III. FREE FLIGHT RMS ERRORS

Response Variable	RMS Error
Roll	0.69 deg
Pitch	0.69 deg
Position	5.86 cm [7.47 6.00 3.38] cm

V. CONCLUSIONS

This work has introduced a CSAM prototype design, which makes use of a coaxial octorotor platform with an offset-mounted 5 DoF manipulator. A quad-core on-board computer running ROS is responsible for all processes not related to flight control: in this case, only manipulator path planning and motion capture communication at present - however this will become more significant in future work as perception sensory is added.

Initial steps have been taken in developing a controller for the system by investigating the effectiveness of an off-the-shelf PID flight control implementation. Position-hold flight testing has shown that the performance metric, RMS position error, degraded from 3.27 cm to 5.86 cm due to movement of the arm. This was found to be due mainly to inertial effects, rather than the change in center of mass; therefore performance could be improved by controlling the arm with a smoother trajectory. Furthermore, the overshoot in roll and pitch responses and oscillatory position response has suggested the need for further tuning, which is also expected to improve performance. Nevertheless, the success criteria outlined previously has been met, even without further tuning – this means it would be possible for the arm to tracks and couple with a branch for sampling.

Future work will follow on from these experiments by analyzing the remaining dynamic phases of branch coupling and decoupling under PID control. This will be done for a range of branch parameters, thus covering the range of possible interaction dynamics to ensure robustness.

REFERENCES

[1] I. Palunko, P. Cruz, and R. Fierro, "Agile Load Transportation : Safe and Efficient Load Manipulation with Aerial Robots," *IEEE Robotics & Automation Magazine*, vol. 19, pp. 69-79, 2012.

[2] P. Pounds and A. Dollar, "Aerial Grasping from a Helicopter UAV Platform," in *Experimental Robotics*. vol. 79, O. Khatib, V. Kumar, and G. Sukhatme, Eds., ed: Springer Berlin Heidelberg, 2014, pp. 269-283.

[3] F. A. Goodarzi, D. Lee, and T. Lee, "Geometric control of a quadrotor UAV transporting a payload connected via flexible cable," *International Journal of Control, Automation and Systems*, vol. 13, pp. 1486-1498, 2015.

[4] K. Alexis, C. Huerzeler, and R. Siegwart, "Hybrid predictive control of a coaxial aerial robot for physical interaction through contact," *Control Engineering Practice*, vol. 32, pp. 96-112, 11// 2014.

[5] M. Fumagalli, R. Naldi, A. Macchelli, R. Carloni, S. Stramigioli, and L. Marconi, "Modeling and control of a flying robot for contact inspection," in *Intelligent Robots and Systems (IROS), 2012 IEEE/RSJ International Conference on*, 2012, pp. 3532-3537.

[6] F. Ruggiero, M. Trujillo, R. Cano, H. Ascorbe, A. Viguria, C. Peréz, *et al.*, "A multilayer control for multirotor UAVs equipped with a servo robot arm," in *2015 IEEE International Conference on Robotics and Automation, Seattle, WA, USA*, 2015.

[7] M. Orsag, C. Korpela, S. Bogdan, and P. Oh, "Hybrid Adaptive Control for Aerial Manipulation," *J. Intell. Robot. Sys.*, vol. 73, pp. 693-707, 2014.

[8] M. Orsag, C. Korpela, S. Bogdan, and P. Oh, "Valve turning using a dual-arm aerial manipulator," in *Unmanned Aircraft Systems (ICUAS), 2014 International Conference on*, 2014, pp. 836-841.

[9] S. Kim, S. Hoseong, and H. J. Kim, "Operating an unknown drawer using an aerial manipulator," in *Robotics and Automation (ICRA), 2015 IEEE International Conference on*, 2015, pp. 5503-5508.

[10] R. Mebarki and V. Lippiello, "Image-Based Control for Aerial Manipulation," *Asian Journal of Control*, vol. 16, pp. 646-656, 2014.

[11] S. Kim, H. Seo, S. Choi, and H. J. Kim, "Vision-guided aerial manipulation using a multirotor with a robotic arm," *Mechatronics, IEEE/ASME Transactions on*, vol. PP, pp. 1-1, 2016.

[12] J. R. Kutia, K. A. Stol, and W. Xu, "Canopy sampling using an aerial manipulator: A preliminary study," in *Unmanned Aircraft Systems (ICUAS), 2015 International Conference on*, 2015, pp. 477-484.

[13] K. Suseong, C. Seungwon, and H. J. Kim, "Aerial manipulation using a quadrotor with a two DOF robotic arm," in *IEEE/RSJ International Conference on Intelligent Robots and Systems*, 2013, pp. 4990-4995.

[14] M. Orsag, C. Korpela, S. Bogdan, and P. Oh, "Lyapunov based model reference adaptive control for aerial manipulation," in *Unmanned Aircraft Systems (ICUAS), 2013 International Conference on*, 2013, pp. 966-973.

[15] P. E. I. Pounds and A. M. Dollar, "Stability of helicopters in compliant contact under PD-PID control," *IEEE Transactions on Robotics*, vol. 30, pp. 1472-1486, 2014.